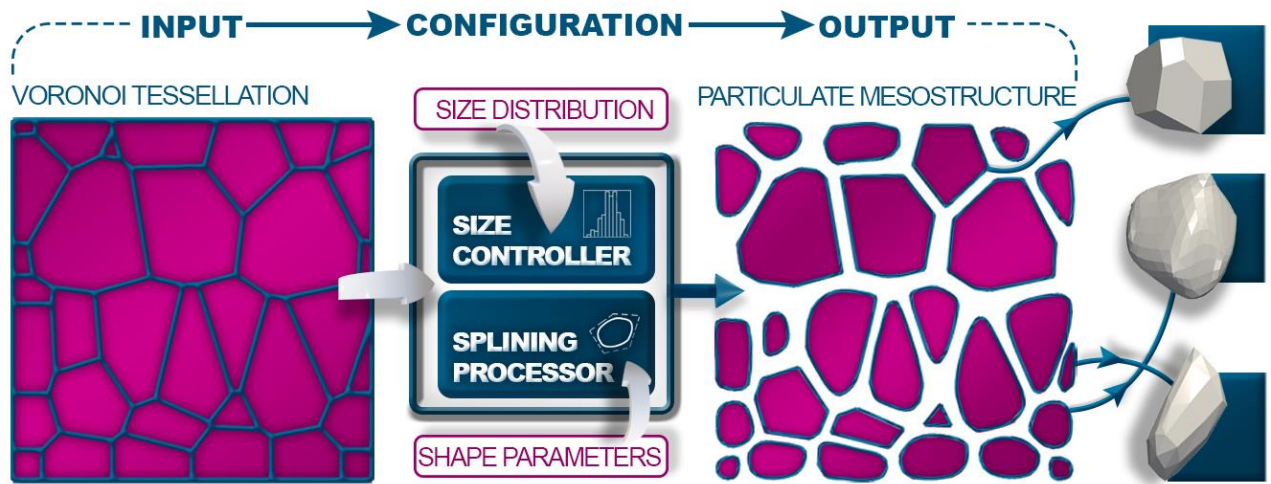


Graphical abstract



An integrated framework for modelling virtual 3D irregulate particulate mesostructure

Sadjad Naderi, Mingzhong Zhang*

*Department of Civil, Environmental and Geomatic Engineering, University College London,
London WC1E 6BT, UK*

Abstract: Many particulate composites show heterogenous mesoscopic structural behaviour due to a random distribution of irregular shaped particles with different sizes ranging from micro to macro scale. Accurate mesoscale models are required to represent actual geometric properties of such a composite with realistic features. In this paper, a cost-effective simulation framework is presented, which can virtually generate three-dimensional mesostructure models composed of irregulate particles with real characteristics. A MATLAB code is developed based on the Voronoi tessellation method and the splining technique. The hybrid Voronoi-spline algorithm can be programmed to control the shape and size of particles based on the experimental data. The examples demonstrated the proper adjustability of the models in accordance with the sieve analysis and shape parameters such as sphericity and roundness. The generated model as a triangulated geometry surface can be directly exported into computational analysis of materials, which uses other numerical techniques including finite element method.

Keywords: Concrete; Geological particles; Aggregates; Voronoi tessellation; Finite element analysis

1 Introduction

Some composites consist of geological particles such as sand, falling rock, gravel, cement particles and aggregates [1-4]. The previous studies have shown that the shape of these particles plays a key role in the physical properties like mechanical performance, workability and durability of the composites [5]. Besides, composites have multiscale characteristics due to different sizes of particles varying from micro/sub-micro to macro scale [6]. To evaluate these mesoscopic properties, a mesostructure model as a crucial part of an analysis is required to represent both realistic shape and size of particles. In general, two computational methods are employed to simulate the particulate structures. The first is the image-based method that replicates a mesostructure by scanning an actual sample using advanced imaging techniques [7-9]. The digital image approaches can help reconstruct an accurate realistic model, but they are restricted by the image resolution. Moreover, such the method produces only one model with a high computational cost. On the contrary, the second approach virtually generates several models and computationally cost lower. The method of virtual fabrication for mesostructure has been broadly utilized to characterize mesoscopic structural properties [10-13]. Several model approaches are frequently proposed, such as lattice models [14, 15], random aggregate model [10, 16], and random particle models [17, 18]. The computational efficiency of these methods mainly depends on the complexity of the algorithms implemented. The difficulties are normally

* Corresponding author. E-mail address: mingzhong.zhang@ucl.ac.uk (M. Zhang)

resulted from the ways of: (1) *Parking*: particles are placed in a domain with the purpose of *no-intersection* during the reconstructing process requiring many complex loops of computation; (2) *Shape description*: simple morphologies (e.g. spheres, ellipsoids and polyhedrons) reduce the volume of computations considerably, but the accuracy level is deducted too. Sometimes the irregular particle models are acquired from an image processing and then virtually parked into the structure [19]. This model is still incorporated into the complex image analysis process and makes the random particle parking more complicated; and (3) *Size control*: the adjustment mechanism becomes more difficult when the irregular particles are required to be randomly distributed and simultaneously, the size distribution profile should be verified by experimental data.

This work is part of a wider project focusing on modelling of complex structures of various materials. Here, the main objective is to develop novel cost-effective computational simulation tools based on a simple algorithm to quickly reconstruct actual heterogenous particulate structures in a three-dimensional (3D) mesoscale framework. A computer code is programmed in MATLAB composed of different independent configuration modules with the abilities to control shape, size and distribution.

The main concept of the modelling approach stands on the use of Voronoi tessellation method as a discretisation technique. The Voronoi tessellations basically discretise a domain into convex polyhedral subdomains (cells) using an arbitrary set of seed points. Each cell is identified by each seed point, consisting of all points closer to that seed than any other [20]. In a 3D tessellated domain with N seed points, the i -th Voronoi cell can be mathematically expressed as:

$$\{R_{P_i}\} = \{x \in \mathfrak{R}^3: \|\mathbf{P}_i - \mathbf{x}\| \leq \|\mathbf{P}_j - \mathbf{x}\|\} \quad (1)$$

$j = 1, 2, \dots, \text{total number of seed points}; j \neq i$

where \mathbf{P}_j is the position of the j -th seed points, R_{P_i} is the cell associated with the position \mathbf{P}_i , and \mathbf{x} is the position of a generic point in \mathfrak{R}^3 .

The Voronoi tessellations are used in various applications in the field of engineering. One of the most common applications is modelling material structures. The digital Voronoi-based materials have been generally developed for polycrystalline materials [21], porous media [22], cellular structure [23] and particulate composites [24]. The variation of applications shows the capabilities of the method in modelling of different morphologies. Besides, the Voronoi tessellation has the advantage of generating statistically representative models with a simple algorithm [25]. Because of these features, an ample range of variability of both shape and size of particles can be generated according to a quantitative shape description. The accuracy of a model is related to the shape description level. The available methodologies similarly describe the particle with the following shape parameters in three levels [6, 26-30]:

- Level I. Proportion of length, height and width:* at the first level, a particle is classified by an overall shape like regular, elongated and flat. Many researchers consider the ellipsoidal geometries to investigate the effect of overall shape on mechanical performance and physical properties of granular materials or particulate composites [31-39].
- Level II. Roundness or angularity:* referring to surface features, some particles can be described as sharp, angular and round. For the particles like aggregates, gravel and crushing stones, the angularity is an important characteristic that significantly influences the strength, friction angle and stability of the material [6]. Studies revealed the importance of local properties of shape (e.g. rounded or sharp edges and corners) on the material's behaviour including tensile strength and dynamic moduli of concrete [40-42].
- Level III. Roughness or smoothness:* it represents the particle surface texture. At this level, the measurement scale is the smallest among the three levels and a particle can be labelled as smooth and rough. Further structural details have been replicated by different approaches, including Voronoi tessellation [43, 44], randomly cutting method [41, 45], randomly growing method [46, 47], and random generation method [16]. All these methods have only proposed the simple convex polyhedral shape. In recent years, the most realistic shapes have been established based on some approaches, e.g. X-ray computed tomography reconstruction [48] and geometrical contraction deformation to simulate non-convex particles [49], and spherical harmonic series to produce single realistic particle [50]. However, as we discussed earlier, it has been always a challenge to keep irregular instinct of mesostructure with a less complication and more control over the shape generation.

In this work, the Voronoi tessellation model is developed to globally or locally control the geometry of particle surface with the shape parameters. Some shape features like roundness are regulated by fitting spline surfaces. The splining technique is a mathematical method normally employed for creating and representing curves and surfaces in computer graphics [51]. It handles a constructed shape with proper flexibility and accuracy. The Loop subdivision surfaces technique is one of the suitable splining methods for complex shapes [52]. The hybrid Voronoi-Spline method is capable of simulating the particles with designated shape effectively. To parametrise a shape, the indices of elongation, sphericity, roundness and convexity are used.

In the following sections, first, the computational methodology to control shape and size of Voronoi cells by systematic design of seed points will be presented. Then, an explanation will be given in detail on the splining process. Afterwards, the approaches to configure size and shape of models will be discussed in depth. For the proposed models, the mesh module available in MATLAB is utilized to triangulate surfaces.

2 Systematic design of seed points

The principle of the Voronoi tessellation method has been mentioned repeatedly in the literature, so we focus more on the extensions proposed. For a comprehensive review, the reference [53] is suggested. Also, some software like *Voro++* [54] individually is available for 3D Voronoi tessellation. Basically, any algorithm produces the data matrix of vertices for each Voronoi cell, can be considered here.

To tessellate a domain, an arbitrary set of points is initially seeded. In the classic Voronoi tessellation, seed points are located at the centre of cells. Shape, size and location of cells are naturally dictated by a system to distribute points. This allows a desired structural attribute to be implemented into a model. Figures 1-3 show the examples including the cubes seeded by different systems and subsequently tessellated to the Voronoi cells with various shape and size distributions. A seeding point system can be strategized either in a part or overall a domain by:

- *irregularity level*: a system is called fully/semi-regular when it generates fully/semi-regular polyhedral shaped cells. This system is normally achieved by a uniform non-random points distribution (e.g. Figure 1a). A random point distribution induces irregularity into the Voronoi tessellation (e.g. Figure 1b or c). An irregularity level can be gradually changed in accordance with a regular system as a reference. The irregularity is systematically raised when the points deviate from the original positions according to the reference. The deviation of seed points can be demonstrated as a displacement vector. If a local polar coordinate system is assumed as its origin is located at the initial position of seed point, then the vector is defined between the origin and the new position of the point. The vector is controlled by three random variables, including the length of vector d and angles θ and φ . The deviation amount is quantified by d which represents the degree of irregularity. To inherently induce irregular attribute into the tessellation, the angles can be randomly generated between 0 and 2π . The irregularity level can be intensified by increasing the length of the vector. It should be noted that the points can only migrate inside the cube. The method to produce new positions can be consistently changed according to any case. For example, the angle θ can be set as a constant against φ as a random variable. To visual comparison, the possible structural evolution is exemplified in Figure 1. The semi-regular shaped cells are distorted by perturbation of points when d increases from (a) to (c). The changes can be quantitatively described by the size of cells or the shape parameters. However, the quantitative comparison is out of the scope of this section.
- *number of seed points*: the average cell size is generally reduced by increasing the number of seed points over the domain. A higher point density in a region results in the smaller Voronoi cell in comparison to other regions in a domain. Figure 2 exemplifies the effect of the number

of points on the cell size. The cube was initially subdivided into 8 equal cubic regions. The greater number of points were seeded in one of the sub-cubes.

- *point coordination*: the seed points can be coordinated by an arbitrary function. As an example, shown in Figure 3, a sinusoid-based function coordinates the seed points and the tessellation. The algorithm firstly generates a data set of points by the sinusoidal function on the plane $z - x$. Afterwards, it triplicates the points on the same plane and repeats the pattern in y -axis direction for 9 more times with the equivalent distance. The generated points are perturbed to create irregular form cells.

In brief, the systematic design of seed points helps to induce the desired attribute into the model and ease the further adjustment of the model. Depending on a case, it can broaden and be combined with different techniques. In this section, we only proposed to show the potential capability of being programmable.

3 Splining process

The splining technique proposed is based on *Loop subdivision surface* method, which was named after *Charles Loop* [55]. This method to create spline surfaces is a standard approximating subdivision scheme for triangle meshes. To the best of our knowledge, the subdivision surface technique has been extensively used in computer graphic design, but we propose to use it in the material model to control shape of particle model. Loop's algorithm mainly consists of two steps: (1) Subdivide a triangulated control mesh of Voronoi cells by quadrisectioning each face and connecting edge midpoints as illustrated in Figure 4a; (2) Update vertex positions as a weighted average of old adjacent positions. The weights assigned to the old vertices are called *masks*. To compute the new geometry, two sets of vertices are updated, i.e., the edge midpoints generated from the previous step and the original vertices. Figure 4b depicts the two types of masks used in Loop's algorithm. The vertex masks applied to an original mesh vertex can be calculated as follows:

$$\alpha = \left(\frac{3}{8} + \frac{1}{4} \cos \frac{2\pi}{n} \right)^2 + \frac{3}{8} \quad (2)$$

$$\beta = \frac{1}{n} (1 - \alpha)$$

where n denotes the number of neighbours.

Therefore, new sets of edge midpoints V_A^* and the original vertices V_{ORIG}^* can be computed from the old original vertices V^O as:

$$V_A^* = \frac{3}{8} (V_B^O + V_C^O) + \frac{1}{8} (V_D^O + V_E^O)$$

$$V_{ORIG}^* = \alpha V_{ORIG}^O + \beta \sum_{i=1}^n (V_{NBR,i}^O) \quad (3)$$

Figure 5 shows the scheme that generates a smoother surface after each iteration. A very smooth surface is reconstructed by increasing the number of subdivision iterations, but it should be noted that the number of triangles made surface increases too. In a finite element analysis, it would increase the number of solid elements and then the computational cost drastically raises. Figure 6 depicts that the splined cells do not intersect the adjacent cells as a spline surface is produced inside a Voronoi cell.

4 Configurations and discussion

The basic techniques to produce Voronoi or splined cells were described so far. Each cell represents primitive surface geometry of a particle. To simulate the actual properties, a model needs to be configured based on the shape and size parameters obtained from the experiments. These parameters are used as numerical inputs. Accordingly, the configuration modules proposed can control local shape and size for each cell or overall properties (e.g. volume fraction of particles). But before, a proper tessellation should be considered as a precondition for model configuration procedure. For instance, a model discretised into small cells might not be easily adjusted to represent coarse particles. The model is firstly configured according to the shapes of cells and then the size.

4.1 Shape configurations

4.1.1 Quantitative description of particle shape

Both seeding points and splining process influence shape of Voronoi cells. These effects on shape variations can be quantitatively described by the shape parameters, including elongation, sphericity, roundness and convexity indices. Elongation E_l and sphericity S_p are mainly used to evaluate the overall shape. Sphericity quantifies the deviation of a particle from a perfect sphere. E_l and S_p can be calculated according to the dimensions from the centre of the cell to the vertices L and the volume \mathbb{V} and surface area \mathbb{S} of the particle respectively as [56]:

$$E_l = \frac{L_{Max}}{L_{Min}} \quad (4)$$

$$S_p = \frac{\text{Surface Area of Equivalent Sphere}}{\text{Surface Area of Particle}} = \frac{4\pi \left(\frac{3\mathbb{V}}{4\pi}\right)^{2/3}}{\mathbb{S}} \quad (5)$$

Volume is computed using the existing function of volume in MATLAB. To implement this function, the cell is meshed by fake solid elements, which are only employed to calculate the volume and are not enclosed into the model. In the next level, the local shape is evaluated by roundness R_n and convexity κ .

Different methods have been used to measure roundness. Based on the approach presented in [1], R_n can be obtained using the angle between the surface position vector \vec{r} and the unit normal vector to the surface \hat{u} . For the triangulated mesh, \vec{r} is interpreted as a vector that connects the cell centre to centre of a triangle element on the surface and \hat{u} is the corresponding normal surface. The angles between \vec{r} and \hat{u} is obtained by $\hat{r} \cdot \hat{u}$, where $\hat{r} = \vec{r}/|\vec{r}|$. Therefore, roundness R_n is defined as:

$$R_n = \frac{\int_{\mathbb{S}} |\hat{r} \cdot \hat{u}| d\mathbb{S}}{\int_{\mathbb{S}} d\mathbb{S}} \xrightarrow{\text{Numerical Format}} R_n = \frac{\sum_{i=1}^m |\hat{r}_i \cdot \hat{u}_i| \Delta \mathbb{S}_i}{\mathbb{S}} \quad (6)$$

where $\Delta \mathbb{S}_i$ denotes the surface area of $i - th$ triangular element and m is the total number of elements.

Concave surfaces might be created after the splining process. To evaluate this feature, the degree of convexity κ is used, which is commonly obtained by the ratio of the volume of the particle \mathbb{V} to the volume of convex hull \mathbb{V}_{CH} [57] generated by the same vertices as the following equation [58]:

$$\kappa = \frac{\mathbb{V}}{\mathbb{V}_{CH}} \quad (7)$$

where \mathbb{V}_{CH} is computed by the function of `convhull` in MATLAB.

All the indices change in a range between 0 and 1 and they are equal to 1 for a sphere. It is noteworthy that the definitions proposed can be replaced by other methods which are more consistent with the case study.

4.1.2 Effect of splining process on unit cell

In this section, the transformation of the Voronoi cells is described during the splining process using the shape parameters. To analyse the effect of Loop subdivision surface on shape characteristics, two original Voronoi cells are typified based on irregularity level of the overall shape. The candidate geometries are likely produced by the algorithm of tessellation with different setups. The first is named *Low-Poly-Sphere (LPS)*, which represents a more rounded geometry with values of elongation and sphericity indices closely equal to 1. Contrarily, the second is called *Almond*, which portrays a high irregular geometry elongated in a direction. The models and corresponding measurements are presented in Table 1. The shape parameters are measured in four levels of Loop subdivision surface. The original Voronoi cells are used as the shape references. The LPS-Voronoi cell model has E_l and S_p that are 50% lower and 15% higher, respectively, than the Almond-Voronoi cell.

As seen in Table 1, most changes are seen after the first iteration. They are more significant for the Almond series where S_p increases 9%. The Voronoi cells are generally reconstructed to a rounded shape geometry. But the values of E_l show that the Almond model is 3% more elongated in contrast to the LPS model, which is truncated about 6%. Regarding local shape features, the roundness values raise about 4% as anticipated for both types. The overall shapes after the splining process look convex, but the values of κ reveal that the convexity locally decreases about 1.5 % due to the small concave surfaces (see Table 1). It is noteworthy that even this amount of concavity would have significant influences on some applications. For instance, it was revealed that the concave feature affected the volume fraction of the interfacial transition zone around the non-convex aggregates with respect to the convex particles in a fully graded concrete [49]. For the second iteration and after, the further shape changes are limited to the small amounts, not more than 2%. The parameters tend to the specific

values, which restrict the shape adjustment procedure. Elements number quadruples after each iteration. It should be noted that the increment of the triangle element number drastically increases the computational cost if the model is meshed by solid elements in any further finite element analysis. Considering small changes of shape associated with high computational volumes, a cost-effective configuration should be proportionately chosen based on the accuracy level expected.

In summary, the splining process changes the Almond type more than LPS cell and sphericity and roundness more than other shape parameters. The overall shape is mainly influenced by Voronoi tessellation method and it is then regulated via Loop subdivision surface technique. As we discussed earlier, the cells can be systematically shaped by different seed points schemes. For example, a model like Figure 1a generates the cells with a higher S_p as compared to Figure 1b or c. A variety of particles are replicated using the shape configurations approach proposed. As a case in point, an original Voronoi cell can represent an aggregate with sharp edges and corners like crushed rock. Or a splined cell can imitate a particle with rounded edges and blunt corners such as gravel.

4.1.3 Examples

A model as an example is used to show how particle shape distribution with reference to sphericity can be uniformly changed after applying the splining technique to all cells. To generate such a model, a unit cube is tessellated using 200 random seed points uniformly distributed. To modify the average of sphericity, the Voronoi cells are splined with two levels of iteration. The *Voronoi* cells and the *splined Voronoi* cells generated here look similar to the models shown in Figure 6 but with different cell numbers. For both models, the sphericity value of each cell is calculated as explained in Section 4.1.1 using Equation 5. Figure 7a illustrates a typical histogram that represents the number of cells within the ranges of S_p values for the models before and after the splining process. Due to overlapping plots, the histogram related to the splined model is shown in transparent form. It enables better visualization of the histogram plot corresponding to the model before splining and easy comparison between them. Thus, the intersection of the plots is seen in a darker colour. The *probability density function* (PDF) with the normal distribution is plotted in Figure 7b. Two parameters of the normal distribution are the standard deviation of 0.03 and the mean value, which is set as the average of S_p of cells. To plot the histogram and PDFs of the S_p data, MATLAB functions ‘normpdf’ and ‘histogram’ were used. As seen in Figure 7b, the graph is shifted to higher sphericity. The analysis reveals that the setting to tessellate produces the Voronoi cells with an average of sphericity of 0.78. After splining, the modification raises the mean value of S_p up to 10% and the number of cells within the range of 0.8 and 0.9. In this example, the splining process is similarly applied in the entire model. But, an algorithm can be designed to dictate how to apply the splining process in the overall domain and indicate number of Loop subdivision surface iteration required to be assigned for each cell. From this perspective, a group of Voronoi cells are recognised under some conditions referred to structural

properties as prescribed by the algorithm proposed. For instance, the Voronoi cells are splined with one iteration level if their sphericity is less than 0.75; with two iterations level if their volume is greater than 1% of the domain; with three iterations level if their centres are positioned in the upper half of the cube and such similar conditions. In the following, an example will be presented to show a multi-conditional implementation of splining process.

Another model is developed by modifying the seed points system used for the semi-regular Voronoi tessellation shown in Figure 1a. The modifications allow producing two more types of irregular shape, one of which is more elongated, in addition to the semi-regular formed cells. The seed point system is modified by two steps: (1) To induce irregularity in a part of the model, the points in the upper half of the box are perturbed using the technique explained in Section 2 with $d = 0.08 \text{ unit}$; (2) To create irregular-elongated-cells, the z coordinates of the seed points in the middle part of the box ($0.3 < z < 0.7$) are changed as $z^{new} = 0.3 + 0.1(z^{old} - 0.3)$. The method displaces the points closer to the plane $z = 0.3$. The corresponding coordinate system is shown in Figure 8.

The Voronoi tessellation and the procedure to configure the model are illustrated in Figure 8. In the first stage, the Voronoi cells are segmented under three conditions specified as $S_p > 0.85$, $0.75 < S_p < 0.85$ and $S_p < 0.75$. For better visualisation, the cells are shrunk. The method to adjust cell size will be elaborated in Section 4.2. Different splining settings are considered for each segmentation. The Voronoi cells with the highest sphericity are not splined. One level of iteration is applied to the cells with the mid-range of S_p . For the cells in the segmentation of the lowest sphericity, two iteration levels are considered. Three types of particles are separately shown in Figure 8. The models are called LPS and Almond in agreement with the names stated earlier. Here, the particle is said to be Flaky because they have the angular and the elongated shape. The names are based on the qualitative description of shapes not quantitative. However, if required, as we discussed, it is possible to characterize based on the shape parameters as well.

4.2 Size configurations

4.2.1 Scaling

An algorithm to configure size is designed based on the scaling scheme. A cell is scaled according to its centre. The centroid position, C , is obtained from the average of the positions of all vertices and the new positions, V_i^{SCALED} , are computed as the following equation:

$$V_i^{SCALED} = C + q(V_i - C), \quad i = 1: \text{number of cell vertices} \quad (8)$$

where q is the scale factor and must be in the range of 0 to 1 as a unit cell can be only downsized to prevent from overlapping with the neighbouring cells.

Figure 9 shows an example of the shrunk unit cells relative to their original size. For each cell, q can be adjusted based on either cell volume or a characteristic length (e.g. radius of a sphere with a volume like a cell) as below:

$$q = \sqrt[3]{\frac{\textit{Arbitrary Volume}}{\textit{Original Cell Volume}}} \quad \textit{or} \quad \frac{\textit{Arbitrary Length}}{\textit{Original Cell Length}} \quad (9)$$

In a particulate domain, the approach to control q is mainly based on one or two criteria. The first is the total volume of particles and the second is either particle average size or particle size distribution. In total volume-control approach, a constant value of q is simply calculated from the ratio of an arbitrary total volume of particles to the total volume of original cells. It is equally assigned in the overall domain. In average size-control approach, q is individually obtained for each cell according to the mean value. The model adjusted contains the same size particles. Each of these two approaches solely regulates a model with high precision, but if two criteria are considered together, the accuracy level might decrease. As an example, Figure 10 prescribes a configuration algorithm built upon both criteria of total volume and average size. In order to ease the algorithm, the system requires to be more flexible in other ways by applying more constraints on the size properties. For example, mean cell size or total volume fraction should be defined for the algorithm within a reasonable range instead of the constant value. In such a case, the deviation from the desired value shows the accuracy level. If so, the model is first adjusted based on the average size and then the total volume. If the module of average size-control is not able to adjust a cell under the condition of $q < 1$, the cell can be removed or another Voronoi tessellation model is generated. Similarly, if the module of total volume-control or all the procedure fails after the accuracy check, a new set of Voronoi cell is required. It should be noted that re-tessellation does not necessarily mean that performing the process with another set of seed points with the same configuration. If required, the seed points should be redesigned.

4.2.2 Particle size distribution

Particle size distribution indicates what *sizes* or *size ranges* of particles are presented in what proportions in the sample particle group to be measured. Data regarding particle size distribution is required to be analysed in order to set up both systems of seeding points and size configuration. A proper estimation of the total number of seed points allows more freedom to calibrate cell size. The possible number of particles indicates the approximation of total seeding points number. The number of particles for each size can be estimated by dividing the representative volume of a particle to the corresponding total volume. For an irregular particle, representative volume is equal to volume of an identical sphere. The radius of the sphere is used as the size descriptor. If the volume of an irregular particle is equal to V , then an equivalent radius R_{eq} can be obtained from the following equation [59]:

$$R_{eq} = \sqrt[3]{\frac{3V}{4\pi}} \quad (10)$$

Particle size distributions have been traditionally calculated based on sieve analysis results for a variety of particulate composites such as concrete with random aggregates [60]. A sieve analysis demonstrates the mass fraction of particles within each size range to be measured and cumulative distribution constructed. This can be presented by formulas, tables or graphics. Fuller curve as one of the most acceptable curves represents the gradation of aggregates in concrete and it can be simply described by the following equation [61]:

$$\mathcal{P}(d) = 100 \left(\frac{d}{d_{max}} \right)^a \quad (11)$$

where $\mathcal{P}(d)$ is the cumulative percentage passing sieve with aperture diameter d , d_{max} is the maximum size of aggregate particles, and a is the exponent of equation ($a = 0.45 - 0.70$).

To simplify the numerical implementation process, the gradation curve given by (11) is divided into segments. The amount of aggregate, \mathbb{V}_{agg} , within the grading segment $[d_i, d_{i+1}]$ can be obtained as [62]:

$$\mathbb{V}_{agg}[d_i, d_{i+1}] = \frac{\mathcal{P}(d_{i+1}) - \mathcal{P}(d_i)}{\mathcal{P}(d_{max}) - \mathcal{P}(d_{min})} \times \mathcal{P}_{agg} \times \mathbb{V}_{tot} \quad (12)$$

where d_{max} and d_{min} are the maximum and minimum sizes of aggregates, \mathcal{P}_{agg} denotes the volume fraction of aggregate and \mathbb{V}_{tot} is the total volume of the specimen.

As results of the data analysis, minimum and maximum values of volume accepted for the model in each size segment are used in the calibration algorithm. The procedure of configuration is performed according to the following steps:

- First, the cells are uniformly scaled in accordance with the total volume fraction of particles.
- Then, the cells are sorted from the largest to the smallest size.
- Cell volumes are respectively checked to be within the volume segments. The process starts with the grading segment containing the largest size.
- Henceforth, several situations may happen. If the largest cell is smaller than the smallest possible particle, the model is aborted and therefore another model with a coarser set of cells are required. If a cell volume is out of range, the cell is scaled down. If the scale factor is larger than 1, the cell is removed.
- The new volume of the cell is recalculated and subtracted from the total volume of particles within the grading segment. This step continues until the remaining volume is less than the minimum possible volume of a particle in the segment.

- Afterwards, the same scenario is repeated for the next smaller size grading segment and then again for successively smaller size grading segment, until the last particle of the smallest size has been checked.
- For the last segment, if the condition of the total volume is verified and some cells remained unchecked, the extra cells are removed. On the contrary, it is possible that the number of cells is not enough to satisfy the total volume condition in the last segments because, for example, the total number of seed points were not predicted properly. In this state, the whole modelling procedure should be redone with a sufficient number of seed points.
- Finally, the total cell volume is checked again. If the accuracy is not accepted, the procedure goes to another loop restarting from the first step. Based on our results, the error values were mostly less than 2% after three loops for more than 100 models with different configurations.

Figure 11 illustrates a flowchart as an example of a possible sequence of steps for the method. In comparison with previous work, there are some advantages that can increase accuracy and decrease computational cost. The generated model has no overlapping problem even after the calibration process and the algorithm only needs a few iterations. It is worth pointing out that the method mentioned above was proposed for the calibration using sieve analysis data. Although, it can be modified for other types of particle size interpretation. Depending on composite application, the particle size distribution obtained from experiments can be described in different forms like PDF, which defines the possible values of volume (or area) occupied by the samples within each size range. For instance, in the application of biopolymer aerogel [63], the Voronoi seed points were generated based on the measured cell size distribution from the experimental desorption data. The PDFs were used as the measurement data to adjust the size of 2D Voronoi cells. In the following, an example of the size configuration based on sieve analysis will be presented.

4.2.3 Examples

The results of the aggregate sieve analysis for a concrete found in the reference [60] were used to adjust a model to take a size distribution into account. The results of particle size analysis are listed in Table 2 for the aggregates occupying 30% of the concrete volume. The particles are graded in three size ranges of diameter including *coarse* particles from 12.7 to 9.50 mm, *medium* particle from 9.5 to 4.75 mm and *small* particle from 4.75 to 2.36 mm. The approximations of minimum and maximum aggregate number are obtained in each segment as [14, 33], [43, 346] and [59, 475] for *coarse*, *medium* and *small* aggregates, respectively. Then, the total number of seed points can be selected within the range of [116, 854]. To test the adjustability of models, several models are generated with the different number of seed points within the estimated range. The points are seeded with the random-uniform-distribution inside a unit cubic domain. The Voronoi cells are splined with two level iterations. Three models shown in Figure 12 contain 200, 500 and 700 particles representing the lower

limit, the mid-range and the upper limit, respectively. The corresponding diagrams of relative probability denote the ratio of the number of particles with different size segmentations relative to the total number of particles.

Based on the results, the performance of the configuration method is mostly acceptable except for the models with lower than 200 particles and upper than 700 particles. The configuration process fails because, for example, the number of *small* particles increases by raising the total number of cells. On the contrary, the number of *coarse* and *medium* particles decreases to an insufficient amount for the calibration purpose. Therefore, the model is unable to be adjusted. A trend is observed in the graphs of the relative probability when the total number increases. If required, the trend can be statistically parameterised using various possible models with a similar size configuration and efficiently considered in a characterisation study.

5 Exporting geometry

The modelling approach generates a mesostructure made from the triangulated mesh. The data related to the elements and nodes are accessible for each cell. In other words, elements can be identified and labelled according to the needs. Then if necessary, the element and node sets can be defined. This output format is consistent with the setting up process of the model for a finite element analysis. So, the code can export the model as STL file, which is a triangular representation of 3D surface geometry. STL is one of the most accepted formats for the different finite element software package. The mesh modules available in software like ANSYS or ABAQUS are able to generate solid elements with reference to triangulated surfaces by the aid of an appropriate technique. Figure 13 exemplifies a mesostructure model composed of the tetrahedral solid elements. The second phase was made after solid meshing using the surfaces of particles and the walls of the cube.

6 Conclusions

This paper presents a novel integrated framework for modelling 3D mesostructure of materials containing irregular particles, which plays a critical role in the material behaviour. The framework mainly consists of systematic design of seed points, splining process, and shape and size configurations. The systematic design of seed points is the key to dictate the main features of mesostructure into the model. It provides better conditions for further shape and size configurations. The model is constrained in this way, but it is very flexible in other forms. A wide range of complex structures with various shapes of a particle can be replicated because of the programmability of different parts of the framework. Depending on case, the algorithms of the Voronoi tessellation and the configurations are programmed and coupled in accordance with needs. From this perspective, the compatibility of the model with any type of experimental data is very high. Via some examples, the models were successfully calibrated and in good agreement with experiment in terms of shape and size. Few numbers of examples were used to show the adjustability of the models because it was

infeasible to cover all broad possibilities. Besides, this paper was focused to only introduce the main features of the simulation framework. In addition to finite element model, it would be worthwhile to couple this framework with other algorithms like discrete element method to provide more insight regarding the problem of packing density of particles [64].

Virtual concrete has been employed in many case studies. For some applications, such as concrete mix design and optimisation, prediction of concrete fracture, and modelling of heat and mass transfer in concrete, the approach can be especially a useful computer-aided tool. As the code is capable to virtually fabricate particles with desired realistic shape characteristics, optional size and distribution. Here, the values of shape parameters could not be gradually changed and an extension to the model is required for better control of shape. In the frame of a larger project, the code is developed to generate more shape variations with the new shape controllers. The development is focused more on the modelling of particles with concave surfaces and adjusting model to the exact values of the shape parameters such as sphericity and roundness.

Acknowledgments

The authors gratefully acknowledge financial support from the Engineering and Physical Sciences Research Council (EP/R041504/1 and EP/N509577/1) and the Royal Society (IE150587).

References

1. Bullard, J.W. and E.J. Garboczi, *Defining shape measures for 3D star-shaped particles: Sphericity, roundness, and dimensions*. Powder technology, 2013. 249: p. 241-252.
2. Dioguardi, F. and D. Mele, *A new shape dependent drag correlation formula for non-spherical rough particles. Experiments and results*. Powder technology, 2015. 277: p. 222-230.
3. Fang, Q., et al., *Mesosopic investigation of the sand particulate system subjected to intense dynamic loadings*. International Journal of Impact Engineering, 2016. 89: p. 62-71.
4. Jin, L., et al., *Multi-scale analytical theory of the diffusivity of concrete subjected to mechanical stress*. Construction and Building Materials, 2015. 95: p. 171-185.
5. Al-Rousan, T., et al., *Evaluation of image analysis techniques for quantifying aggregate shape characteristics*. Construction and Building Materials, 2007. 21(5): p. 978-990.
6. Yan, P., et al., *3D numerical modelling of solid particles with randomness in shape considering convexity and concavity*. Powder Technology, 2016. 301: p. 131-140.
7. Garboczi, E.J., *Three-dimensional mathematical analysis of particle shape using X-ray tomography and spherical harmonics: Application to aggregates used in concrete*. Cement and concrete research, 2002. 32(10): p. 1621-1638.
8. Latham, J.P. and A. Munjiza, *The modelling of particle systems with real shapes*. Philosophical Transactions of the Royal Society of London. Series A: Mathematical, Physical and Engineering Sciences, 2004. 362(1822): p. 1953-1972.

9. Zhu, W. and C. Tang, *Numerical simulation on shear fracture process of concrete using mesoscopic mechanical model*. Construction and Building Materials, 2002. 16(8): p. 453-463.
10. Xu, W., Z. Lv, and H. Chen, *Effects of particle size distribution, shape and volume fraction of aggregates on the wall effect of concrete via random sequential packing of polydispersed ellipsoidal particles*. Physica A: Statistical Mechanics and its Applications, 2013. 392(3): p. 416-426.
11. Zohdi, T., *Genetic design of solids possessing a random-particulate microstructure*. Philosophical Transactions of the Royal Society of London. Series A: Mathematical, Physical and Engineering Sciences, 2003. 361(1806): p. 1021-1043.
12. Xu, W., et al., *Theoretical estimation for the volume fraction of interfacial layers around convex particles in multiphase materials*. Powder technology, 2013. 249: p. 513-515.
13. Xu, W., et al., *Interfacial effect on physical properties of composite media: Interfacial volume fraction with non-spherical hard-core-soft-shell-structured particles*. Scientific reports, 2015. 5: p. 16003.
14. Schlangen, E. and J. Van Mier, *Experimental and numerical analysis of micromechanisms of fracture of cement-based composites*. Cement and concrete composites, 1992. 14(2): p. 105-118.
15. Liu, L., et al., *Aggregate shape effect on the diffusivity of mortar: a 3D numerical investigation by random packing models of ellipsoidal particles and of convex polyhedral particles*. Computers & structures, 2014. 144: p. 40-51.
16. Wittmann, F., P. Roelfstra, and H. Sadouki, *Simulation and analysis of composite structures*. Materials science and engineering, 1985. 68(2): p. 239-248.
17. Bažant, Z.P., et al., *Random particle model for fracture of aggregate or fiber composites*. Journal of engineering mechanics, 1990. 116(8): p. 1686-1705.
18. Xu, W., et al., *Prediction of transport behaviors of particulate composites considering microstructures of soft interfacial layers around ellipsoidal aggregate particles*. Soft Matter, 2014. 10(4): p. 627-638.
19. Thomas, S., Y. Lu, and E. Garboczi, *Improved model for three-dimensional virtual concrete: anm model*. Journal of Computing in Civil Engineering, 2015. 30(2): p. 04015027.
20. Du, Q., V. Faber, and M.J.S.r. Gunzburger, *Centroidal Voronoi tessellations: Applications and algorithms*. 1999. 41(4): p. 637-676.
21. Sun, Z., R.E. Logé, and M.J.C.M.S. Bernacki, *3D finite element model of semi-solid permeability in an equiaxed granular structure*. 2010. 49(1): p. 158-170.
22. Naderi, S., et al., *Modeling of porosity in hydroxyapatite for finite element simulation of nanoindentation test*. 2016. 42(6): p. 7543-7550.

23. Zhu, H., J. Hobdell, and A.J.A.m. Windle, *Effects of cell irregularity on the elastic properties of open-cell foams*. 2000. 48(20): p. 4893-4900.
24. Wang, X., et al., *Computational technology for analysis of 3D meso-structure effects on damage and failure of concrete*. 2016. 80: p. 310-333.
25. Fritzen, F., T. Böhlke, and E. Schnack, *Periodic three-dimensional mesh generation for crystalline aggregates based on Voronoi tessellations*. Computational Mechanics, 2009. 43(5): p. 701-713.
26. Wadell, H., *Volume, shape, and roundness of rock particles*. The Journal of Geology, 1932. 40(5): p. 443-451.
27. Krumbein, W.C., *Measurement and geological significance of shape and roundness of sedimentary particles*. Journal of Sedimentary Research, 1941. 11(2): p. 64-72.
28. Powers, M.C., *A new roundness scale for sedimentary particles*. Journal of Sedimentary Research, 1953. 23(2): p. 117-119.
29. Barrett, P.J., *The shape of rock particles, a critical review*. Sedimentology, 1980. 27(3): p. 291-303.
30. Chandan, C., et al., *Application of imaging techniques to geometry analysis of aggregate particles*. Journal of Computing in Civil Engineering, 2004. 18(1): p. 75-82.
31. Rothenburg, L. and R.J. Bathurst, *Micromechanical features of granular assemblies with planar elliptical particles*. Géotechnique, 1992. 42(1): p. 79-95.
32. Emeriault, F. and C. Claquin, *Statistical homogenization for assemblies of elliptical grains: effect of the aspect ratio and particle orientation*. International journal of solids and structures, 2004. 41(21): p. 5837-5849.
33. Rothenburg, L. and R.J. Bathurst, *Numerical simulation of idealized granular assemblies with plane elliptical particles*. Computers and geotechnics, 1991. 11(4): p. 315-329.
34. Leite, J., V. Slowik, and J. Apel, *Computational model of mesoscopic structure of concrete for simulation of fracture processes*. Computers & structures, 2007. 85(17-18): p. 1293-1303.
35. Xu, W., et al., *A general micromechanical framework of effective moduli for the design of nonspherical nano-and micro-particle reinforced composites with interface properties*. Materials & Design, 2017. 127: p. 162-172.
36. Xu, W., Y. Wu, and M. Jia, *Elastic dependence of particle-reinforced composites on anisotropic particle geometries and reinforced/weak interphase microstructures at nano-and micro-scales*. Composite Structures, 2018. 203: p. 124-131.
37. Xu, W., Y. Wu, and X. Gou, *Effective elastic moduli of nonspherical particle-reinforced composites with inhomogeneous interphase considering graded evolutions of elastic modulus and porosity*. Computer Methods in Applied Mechanics and Engineering, 2019. 350: p. 535-553.

38. Xu, W., et al., *Multiple-inclusion model for the transport properties of porous composites considering coupled effects of pores and interphase around spheroidal particles*. International Journal of Mechanical Sciences, 2019. 150: p. 610-616.
39. Xu, W., et al., *N-phase micromechanical framework for the conductivity and elastic modulus of particulate composites: Design to microencapsulated phase change materials (MPCMs)-cementitious composites*. Materials & Design, 2018. 145: p. 108-115.
40. Höhner, D., S. Wirtz, and V. Scherer, *A study on the influence of particle shape on the mechanical interactions of granular media in a hopper using the discrete element method*. Powder technology, 2015. 278: p. 286-305.
41. Elmouttie, M., G. Poropat, and G. Krähenbühl, *Polyhedral modelling of rock mass structure*. International Journal of Rock Mechanics and Mining Sciences, 2010. 47(4): p. 544-552.
42. Ma, H., W. Xu, and Y. Li, *Random aggregate model for mesoscopic structures and mechanical analysis of fully-graded concrete*. Computers & Structures, 2016. 177: p. 103-113.
43. Asahina, D. and J. Bolander, *Voronoi-based discretizations for fracture analysis of particulate materials*. Powder Technology, 2011. 213(1-3): p. 92-99.
44. Eliáš, J., *Simulation of railway ballast using crushable polyhedral particles*. Powder Technology, 2014. 264: p. 458-465.
45. De Pellegrin, D. and G. Stachowiak, *Simulation of three-dimensional abrasive particles*. Wear, 2005. 258(1-4): p. 208-216.
46. Fang, Q., et al., *An algorithm for the grain-level modelling of a dry sand particulate system*. Modelling and Simulation in Materials Science and Engineering, 2014. 22(5): p. 055021.
47. Fang, Q. and J. Zhang, *3D numerical modeling of projectile penetration into rock-rubble overlays accounting for random distribution of rock-rubble*. International Journal of Impact Engineering, 2014. 63: p. 118-128.
48. Fityus, S., A. Giacomini, and O. Buzzi, *The significance of geology for the morphology of potentially unstable rocks*. Engineering Geology, 2013. 162: p. 43-52.
49. Xu, W., et al., *Random non-convex particle model for the fraction of interfacial transition zones (ITZs) in fully-graded concrete*. Powder Technology, 2018. 323: p. 301-309.
50. Jia, M., W. Xu, and Z. Zhu, *Numerical study on the excluded volumes of realistic 3D non-convex particles*. Powder Technology, 2019. 349: p. 52-58.
51. Catmull, E. and J.J.C.-a.d. Clark, *Recursively generated B-spline surfaces on arbitrary topological meshes*. 1978. 10(6): p. 350-355.
52. Biermann, H., A. Levin, and D. Zorin. *Piecewise smooth subdivision surfaces with normal control*. in *Proceedings of the 27th annual conference on Computer graphics and interactive techniques*. 2000. ACM Press/Addison-Wesley Publishing Co.

53. Aurenhammer, F., *Voronoi diagrams—a survey of a fundamental geometric data structure*. ACM Computing Surveys (CSUR), 1991. 23(3): p. 345-405.
54. Rycroft, C., *Voro++: A three-dimensional Voronoi cell library in C++*. 2009, Lawrence Berkeley National Lab.(LBNL), Berkeley, CA (United States).
55. Loop, C., *Triangle mesh subdivision with bounded curvature and the convex hull property*. MSR Tech Report MSR-TR-2001–24, 2001.
56. He, H., et al., *On the shape simulation of aggregate and cement particles in a DEM system*. Advances in Materials Science and Engineering, 2015. 2015.
57. Barber, C.B., et al., *The quickhull algorithm for convex hulls*. ACM Transactions on Mathematical Software (TOMS), 1996. 22(4): p. 469-483.
58. He, H., et al., *Shape analysis of fine aggregates used for concrete*. Image Analysis & Stereology, 2016. 35(3): p. 159-166.
59. Xu, W. and Y. Jiao, *Theoretical framework for percolation threshold, tortuosity and transport properties of porous materials containing 3D non-spherical pores*. International Journal of Engineering Science, 2019. 134: p. 31-46.
60. Hirsch, T.J., *Modulus of elasticity of concrete affected by elastic moduli of cement paste matrix and aggregate*. ACI Journal Proceedings, 1962. 59(3): p. 427-452.
61. Wriggers, P. and S. Moftah, *Mesoscale models for concrete: Homogenisation and damage behaviour*. Finite elements in analysis and design, 2006. 42(7): p. 623-636.
62. Wang, Z., A. Kwan, and H. Chan, *Mesoscopic study of concrete I: generation of random aggregate structure and finite element mesh*. Computers & structures, 1999. 70(5): p. 533-544.
63. Rege, A., M. Hillgärtner, and M. Itskov, *Mechanics of biopolymer aerogels based on microstructures generated from 2-d Voronoi tessellations*. The Journal of Supercritical Fluids, 2019. 151: p. 24-29.
64. Xu, W., B. Xu, and F. Guo, *Elastic properties of particle-reinforced composites containing nonspherical particles of high packing density and interphase: DEM–FEM simulation and micromechanical theory*. Computer Methods in Applied Mechanics and Engineering, 2017. 326: p. 122-143.

Notation list

a	Exponent of Fuller equation
C	Position of cell centre
d	Degree of irregularity and deviation distance of seed points
d	Aperture diameter in sieve analysis
E_l	Elongation index
κ	Convexity
L	Dimension from centre to vertex in a cell
m	Number of elements
n	Number of neighbours of a vertex in Loop's algorithm
P	Position of seed points
\mathcal{P}	Cumulative percentage passing sieve
q	Scale factor
R_{eq}	Equivalent radius
R_p	Position of Voronoi cells
\mathfrak{R}^3	Three-dimensional domain
R_n	Roundness
\vec{r}	Surface position vector
S_p	Sphericity
\mathbb{S}	Surface of cell or particle
\hat{u}	Unit normal vector
V	Position of cell vertices
\mathbb{V}	Volume of cell or particle
\mathbb{V}_{CH}	Volume of convex hull
x	Position of a generic point
α, β	Vertex masks in Loop's algorithm
θ, φ	Deviation angles of seed points

Figures

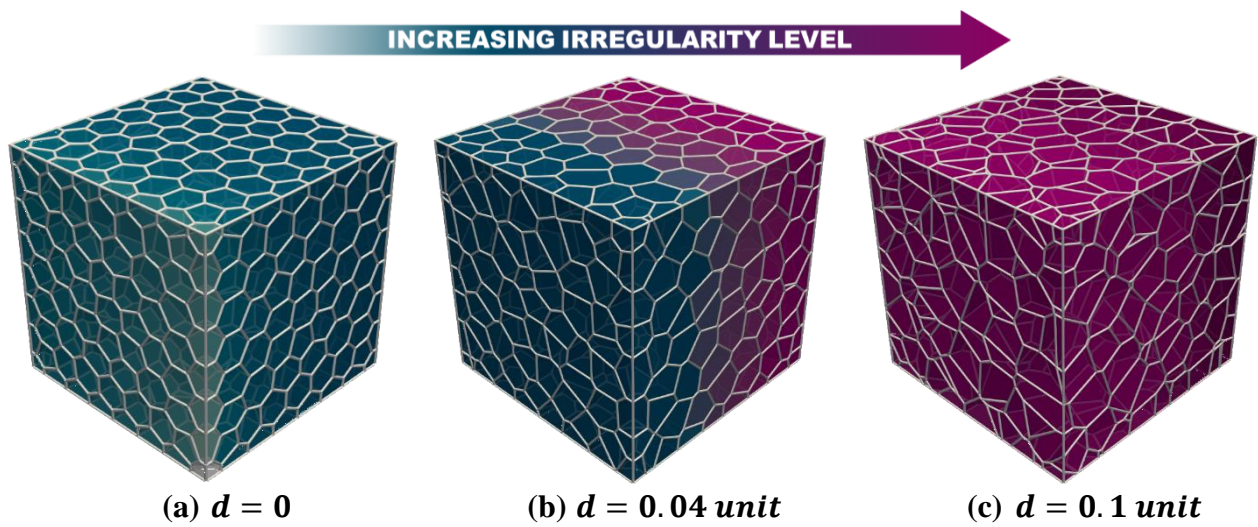


Figure 1. Semi-regular shape of Voronoi cells (a) transformed to irregular shape (b and c) by increasing displacement, d , representing the deviation of seed points from the original position according to the model (a).

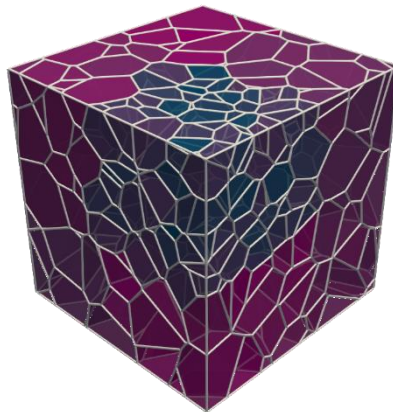


Figure 2. Generation of smaller Voronoi cells in a part of the model through increasing number of points.

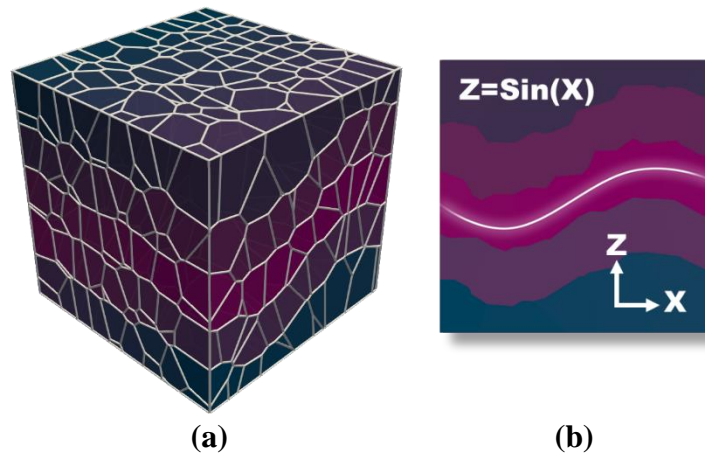


Figure 3. (a) Cube tessellated by the seed points coordinated using a sinusoid-based function; (b) A schematic illustrates how the structural attribute is affected by the proposed function.

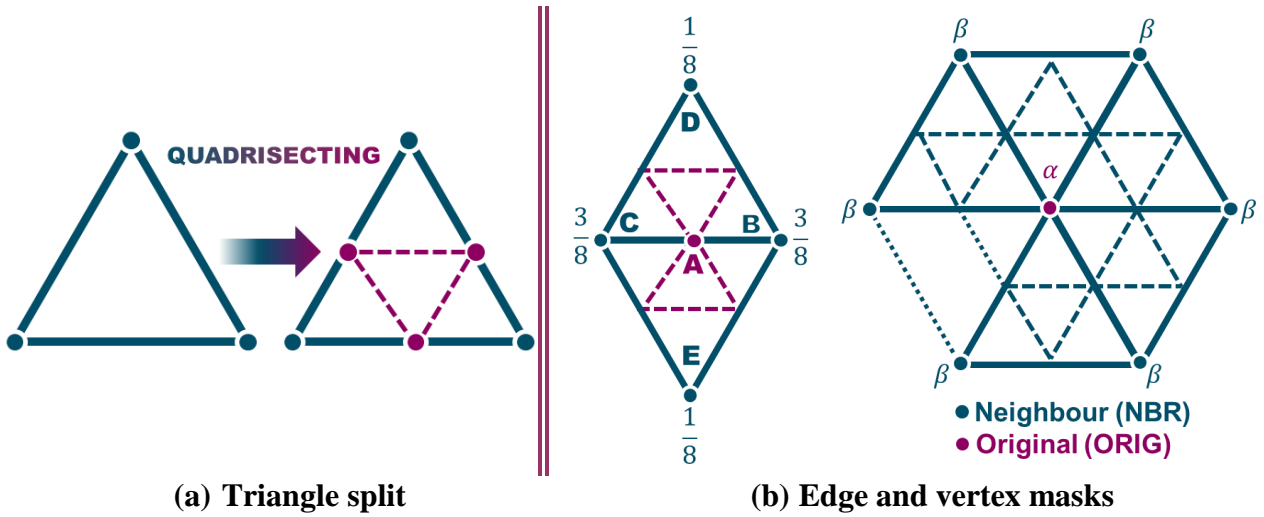


Figure 4. Two main steps in Loop subdivision scheme.

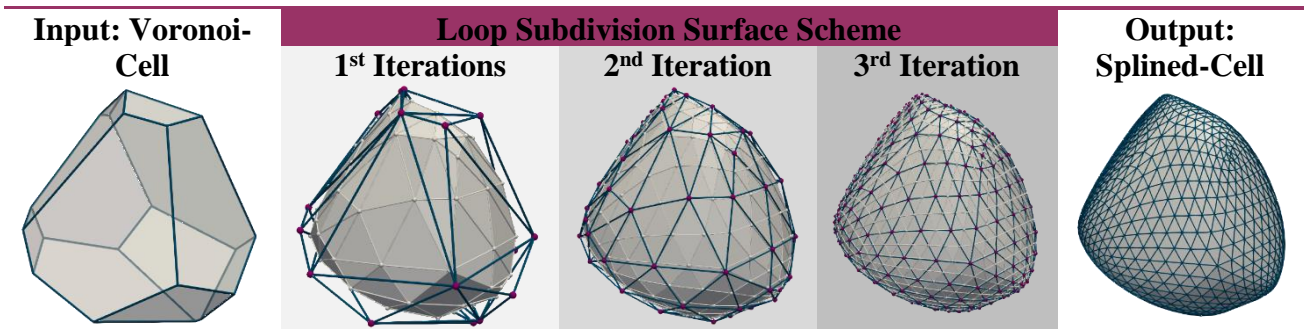


Figure 5. Shape transformation of the polygonal Voronoi cell through the subdivision surface procedure after three iterations. In each iteration, the control points and their connectivity are restructured by the geometry in the previous step.

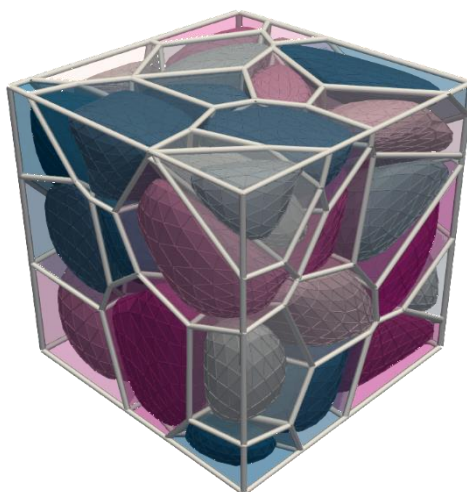


Figure 6. Splined cells produced inside Voronoi cells (in transparent from) with no intersection with the adjacent cells after two iterations.

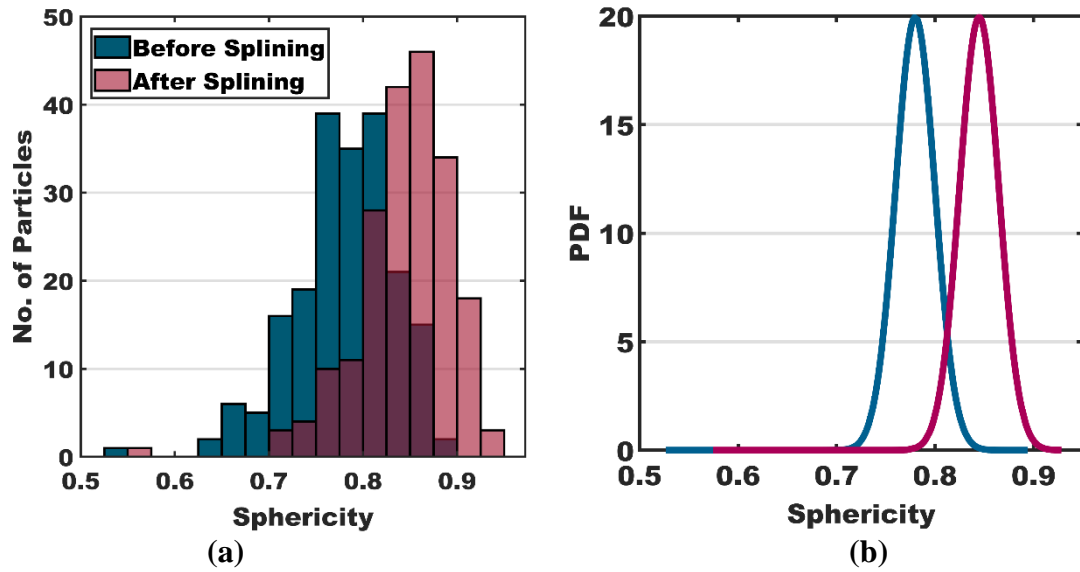


Figure 7. To demonstrate the transformation through the splining process, two models are compared. The first model is generated by tessellation with 200 seed points which are randomly and uniformly distributed. The second model is produced by splining the Voronoi cells of the first model. The cell shape distribution based on sphericity before and after the splining process is shown. (a) The histograms illustrate the number of cells within the ranges of S_p . The histogram plot related to splined cells is displayed in transparent form. (b) the PDFs with the normal distribution are plotted with the mean equals to the average of S_p and standard deviation of 0.03.

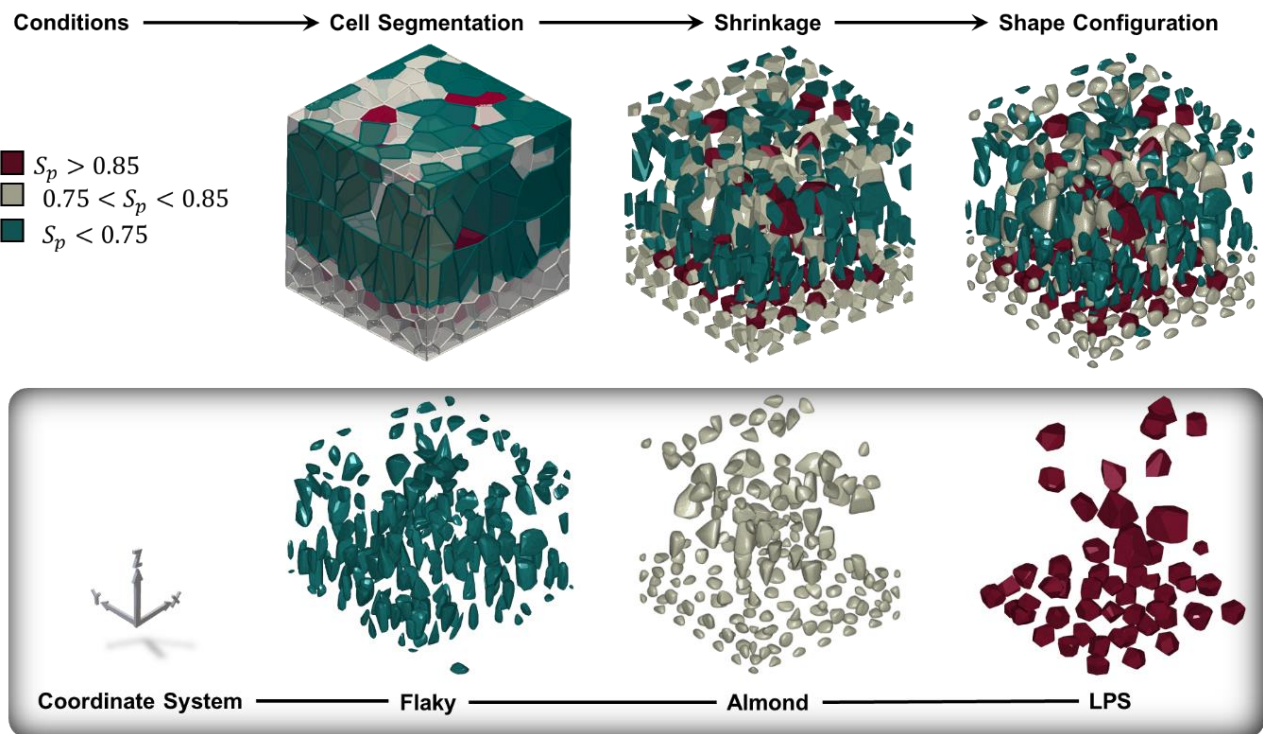


Figure 8. Three types of shapes including LPS, Almond and Flaky produced in the model and illustrated in the lower row. Voronoi cells are segmented under the conditions based on sphericity of the original Voronoi cells to configure the shape. After shrinking the cells, the splining technique is applied to each segmentation with different settings.

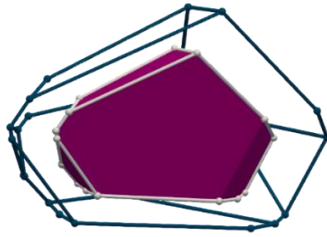


Figure 9. Unit cell scaled down relative to the original Voronoi cell relative to the centre.

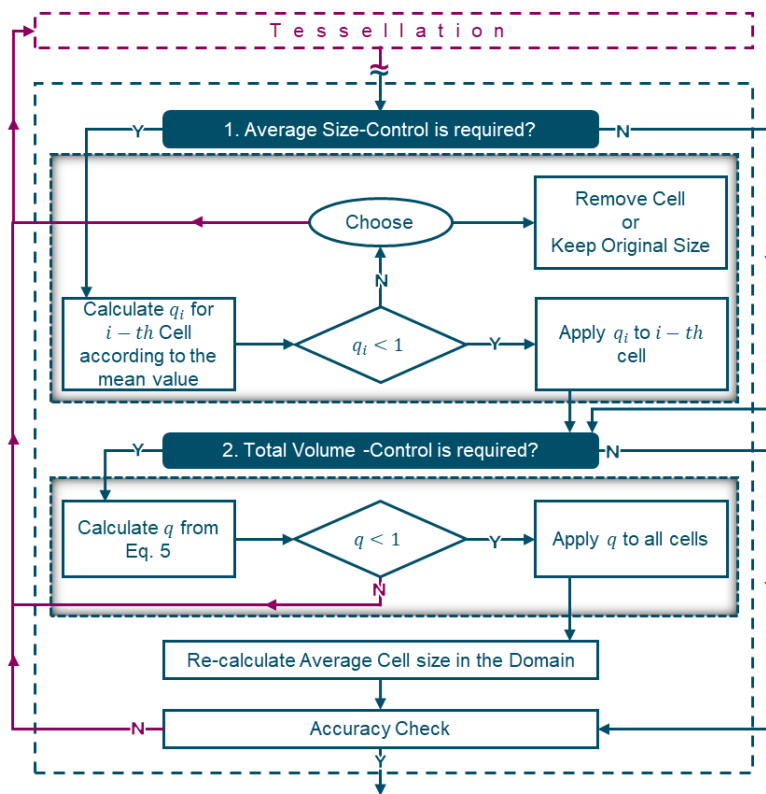


Figure 10. A flowchart of size configuration system referring to total volume and average size of particles.

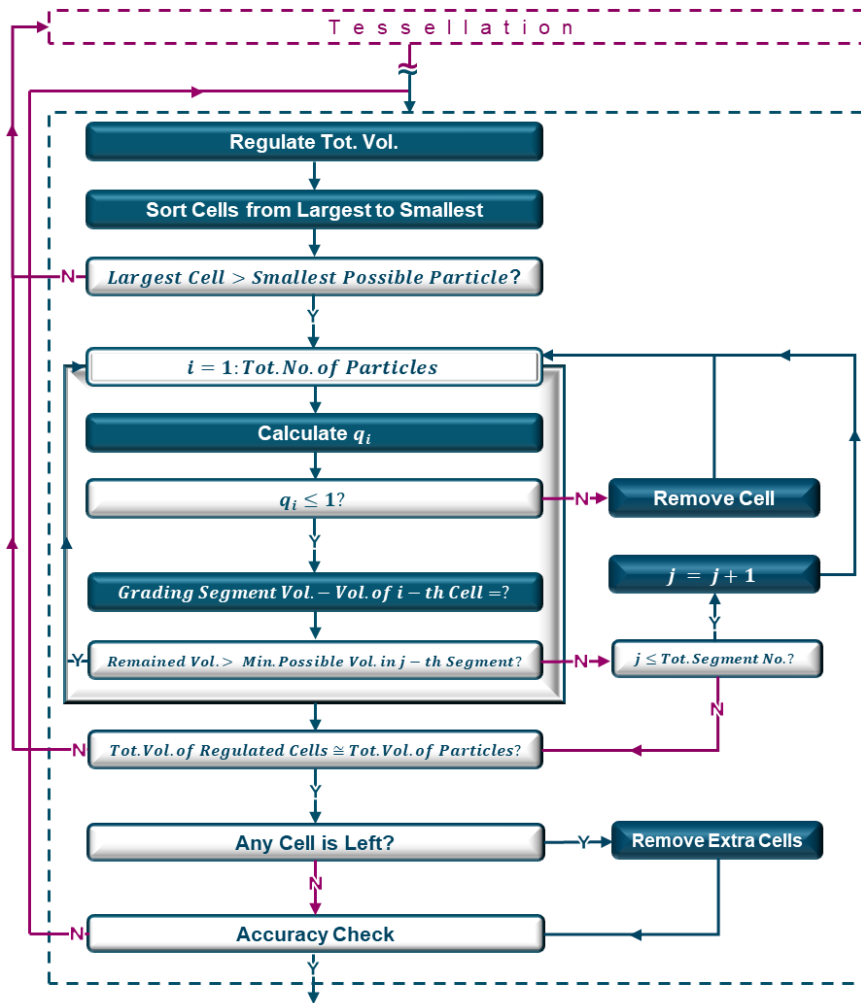


Figure 11. A flowchart as an example of size configuration method based on particle size distribution data obtained from sieve analysis test.

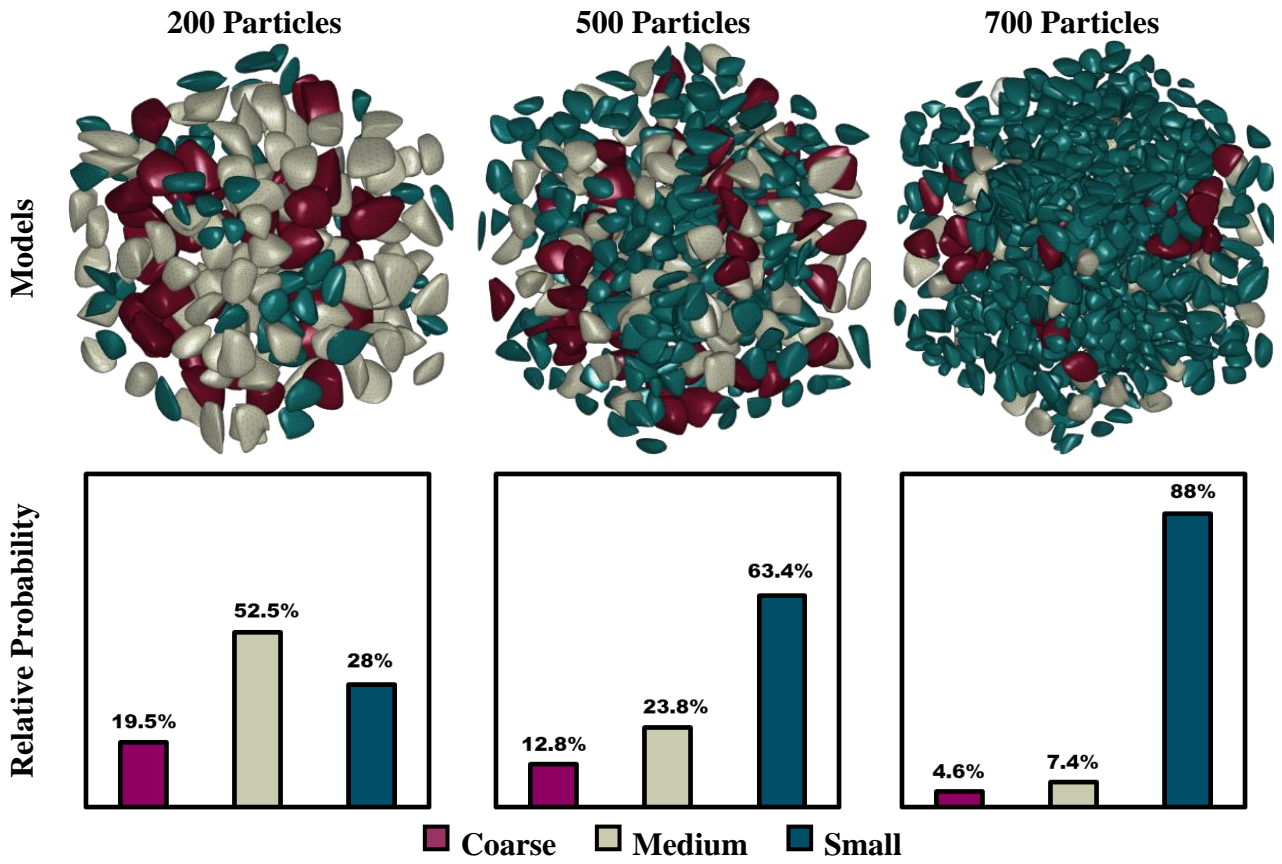


Figure 12. Relative probability representing the ratio of the number of particles within each size segment to the total number of particles. The aggregates with 30% density per the cubic unit of concrete are calibrated according to the sieve analysis for three different sizes.

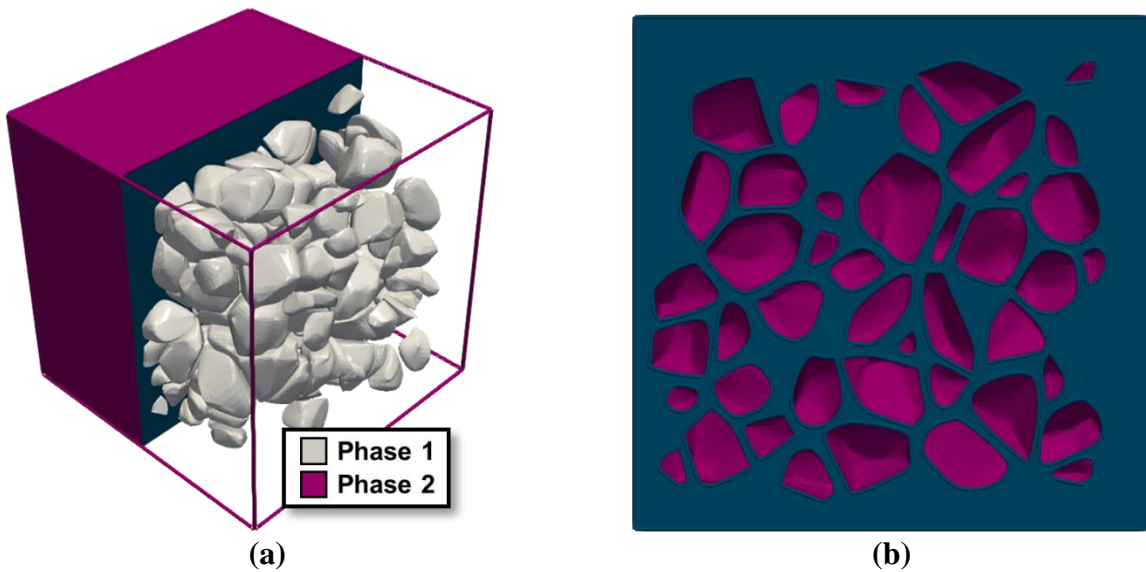


Figure 13. (a) The model including two phases meshed by solid elements and shown in the cross-sectional view. (b) Cross-section of the second phase presented in the absence of the particles (the first phase).

Tables

Table 1. Shape parameters for two types of Voronoi cells including Low-Poly-Sphere (LPS) and Almond models measured for the original Voronoi cells in four levels of splining. The values listed in the upper and the lower rows for each parameter belong to LPS and Almond models, respectively.

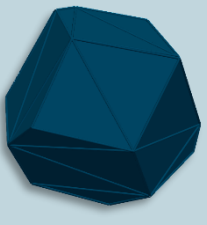
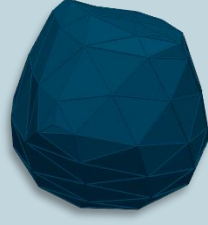
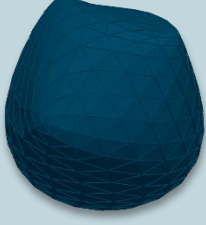
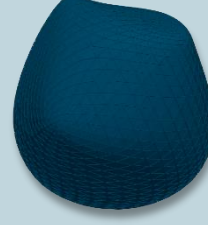

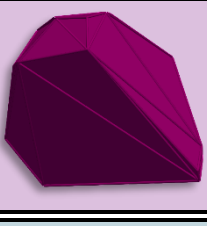
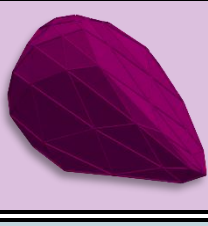
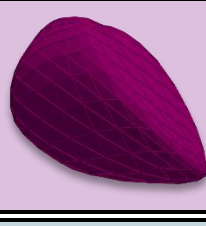


	Voronoi Cell	1 st Iteration	2 nd Iteration	3 rd Iteration	4 th Iteration
LPS					
Almond					
E_l	1.537 3.098	1.450 3.190	1.453 3.479	1.454 3.516	1.455 3.541
S_p	0.9035 0.7681	0.9543 0.8382	0.9664 0.8546	0.9689 0.8577	0.9696 0.8588
R_n	0.9207 0.7584	0.9570 0.7939	0.9652 0.8054	0.9669 0.8078	0.9673 0.8084
κ	1 1	0.9869 0.9848	0.9919 0.9890	0.9924 0.9888	0.9927 0.9895

Table 2. Particle size distribution of coarse aggregate in concrete [51]

Sieve size (mm)	Total percentage retained (%)	Total percentage passing (%)	Total volume (mm ³)
12.7	0	100	1072.5
9.50	39	61	448.92
4.75	90	10	56.11
2.36	98.6	1.4	6.88